Linear augmented cylindrical wave Green's function method for electronic structure of nanotubes with substitutional impurities

P. N. D'yachkov, D. Z. Kutlubaev, and D. V. Makaev*
Kurnakov Institute of General and Inorganic Chemistry, Russian Academy of Sciences, Leninskii pr. 31, 119991 Moscow, Russia
(Received 6 May 2010; revised manuscript received 25 June 2010; published 19 July 2010)

A first-principles numerical method for calculation of the electronic structure of the point impurities in the single-walled carbon nanotubes (SWNTs) based on a Green's function technique is developed. The host SWNTs electron Green's function is calculated using a linear augmented cylindrical wave theory. The Green's function of the impurities is calculated in the terms of matrix Dyson equation. The impurities are described by the single-site perturbed muffin-tin potentials in otherwise perfect nanotubes with the rotational and helical symmetries. Due to the account of these symmetry properties, the method is developed applicable to any tubule including the chiral SWNTs with point defects independent of the number of atoms in translational unit cell of the host systems. We give results for the local densities of states (DOSs) of the boron and nitrogen impurities in the metallic (7,7), (5,5), and (10,10) semimetallic (8,2) and (9,6), and semiconducting (13,0), (12,2), (11,3), (10,5), (8,7), and (10,0) SWNTs, as well as in the polyynic and cumulenic carbynes. It is shown that the boron and nitrogen defects do not destroy the metallic character of electronic structure of the armchair tubules. An increase in the DOS in the Fermi energy region is the most significant effect of boron and nitrogen dopants in the case of metallic and semimetallic SWNTs. In all the semiconducting SWNTs, in the vicinity of optical gap, there is a drastic difference between the effects of the boron and nitrogen impurities. The boron-related states close the gap of the perfect tubules. In the gap region, the effects of nitrogen atom are restricted with a minor growth of the local DOSs just below and above the Fermi energy. Beyond the Fermi-energy region up to the *s* bottom of the valence bands, the effects of impurities are similar in all the tubules. As one goes from carbon to the boron, the local DOS decreases, and the peaks almost disappear, but the nitrogen local DOS is somewhat greater than that of the carbon. In the semiconducting polyynic carbyne, the boron and nitrogen defects close the gap between the valence and conduction bands. In the case of metallic cumulenic carbine, if the boron or nitrogen atom takes the place of carbon, the local DOS at the Fermi level increases.

DOI: 10.1103/PhysRevB.82.035426 PACS number(s): 73.22.−f, 73.63.Fg

I. INTRODUCTION

In their simplest form, the defect-free single-walled carbon nanotubes (SWNTs) are the hexagonal networks of covalently bound carbon atoms in various cylindrical structures. The SWNTs with perfect honeycomb carbon arrangements have emerged as the attractive materials for molecular electronic applications because the SWNTs can be either one-dimensional metals, semiconductors, or even quantum wires depending on their diameter and chirality.[1–8] Based on the SWNTs, the single-electron and field-effect transistors, chemical sensors, emission, electromechanical, and electromagnetic devices have been realized experimentally.[9–17] Carbon nanotubes are famous for their almost perfect structure; the high-quality SWNTs are confirmed to contain only one defect per 4 μm on average.[18] However, some defects are still present in the SWNTs. The SWNTs may have various atomic-scale point defects such as the vacancies, impurities, and adatoms on the tubules walls, kinks, junctions, as well as the different topological defects such as pentagon-heptagon pairs, all of which can appear during the nanotube growth or can be created by external action. The ion, electron, and light irradiations are successful in creating individual atomic-scale nanotube vacancies;[19–22] it has been suggested to dope nanotubes with the H, B, and N atoms using the ion irradiation too.[23] The experimental reversible creation and annihilation of defects on the SWNTs with the tip of a scanning tunneling microscope (STM) have been reported.[24] The presence of structural defects results in a change in the SWNTs electronic-structure, transport properties, optical absorption, specific heat, magnetic susceptibility, and even a single defect can have tremendous electronic effects in one-dimensional conductors.[25,26] A local modification of the electronic structure of carbon nanomaterials is important for development of the carbon-based nanoelectronics. Particularly, the point defects in the SWNTs can act as the gate-tunable electron scatters, and SWNTs with defects can be the basis for new types of electronic devices.[9,26] Inducing defect sites in the SWNTs structure may give rise to complex functional devices such as single-electron transistors operable at room temperature.[10] The defects can control the operation of nanotube-based chemical sensors.[27] Moreover, the defects can impede the adsorption of quantum gases inside a bundle of carbon nanotubes[28] and give rise to irradiation-mediated pressure buildup inside nanotubes.[29] The defective nanotubes could be used as catalysts, and could facilitate thermal dissociation of water.[30] The dangling bonds of vacancy can provide active sites for atomic absorption or serve as a bridge of chemical connection between two tubes. Finally, the structural defects play a major role in toxicity of the nanotubes.[31]

Understanding how imperfections influence the electronic behavior of materials is of fundamental importance. The nonideal nanotubes are therefore intensively studied. In individual metallic SWNTs, defects can be successfully characterized by transport measurements and scanned gate microscopy because a resonant electron scattering by defects in the

nanotube is varied by the gate voltage.[25] STM and scanning tunneling spectroscopy (STS) are the methods which provide direct information both on atomic and local electronic structure of the carbon nanotubes.[32,33] Defects are easily detected in Raman spectroscopy because they break the symmetry of the SWNT, relax the momentum conservation rules that govern Raman-scattering processes, and locally stiffen the lattice. These spectra can be used to differentiate between positively and negatively charged defects. It also reveals that phonons and electrons associated with doped tubes behave differently from their brethren in unperturbed carbon nanotubes.[34,35] In the individual SWNT, using a selective electrochemical method, one can label the point defects and make them easily visible for quantitative analysis; a sequence of electrochemical potentials applied to SWNT can selectively nucleate a metal deposition at the sites of highest chemical reactivity.[18] The signatures of defects can be detected with x-ray photoelectron spectroscopy by monitoring changes in the 1*s* C peak shape, which is sensitive to the type of carbon bonding, and with the electron-spin-resonance method.[36]

The foundation stones of the SWNTs defects electron-structure theory were laid down more than 10 years ago in the terms of the π-electronic tight-binding studies.[37–43] The calculations based on the first models have shown that structural defects in the underlying carbon lattice can substantially modify the electronic properties of SWNTs due to the formation of the defect states and resonant electron scattering at corresponding energies. For example, it was predicted using the tight-binding π-band approximation with surface Green's function matching method that introduction of isolated pentagon, heptagon, or the single pentagon-heptagon pair defects into the hexagonal network of the SWNT can change the helicity of the tube and result in a formation of nanoscale metal/semiconductor or semiconductor/semiconductor junctions.[38,44] The tight-binding recursion model has shown that the one, two, and three pentagon-heptagon pair topological defects in the hexagonal network of the SWNTs form resonant states (sharp peaks) in the density of states (DOS) and govern the electronic behavior around the Fermi level (E_F).[37] Similar approach shows that a pure carbon quantum dot can be designed by introducing several pentagon-heptagon defects in the SWNTs and predicts the energies of discrete levels in these systems.[39] According to the tight-binding supercell data, the topological bond rotation (Stone-Wales) defects close the gap in large-gap SWNTs, open the gap in small-gap nanotubes, and increase the DOS in metallic tubules.[40] For the simplest possible defect, a single vacancy, the quantum conductance was calculated as a function of tube radius within the Landauer formalism in the π-tight-binding scheme.[39,45–47] Investigated in the terms of the π-electronic recursion and Green's function approach, the calculated DOS and STS images of both metallic and semiconducting SWNTs predict the vacancy-induced states at the Fermi energy and hillocklike features in the atomically resolved STM images.[48,49] The π-tight-binding transfer-matrix method was used to calculate the reflection coefficient for a barrier created by point defects in the armchair and zigzag SWNTs.[42,43] The π-electronic and transport properties of the SWNTs with defects were also studied within a $\mathbf{k}\cdot\mathbf{p}$ scheme and Green's function scattering formalism for a model strong short-range potential.[50,51] The result obtained in this scheme are shown to agree essentially with the tight-binding models.[51,52]

Going beyond the π-electron theory, the effects of vacancies, substitutional boron, or nitrogen impurities, and local topological defects on the DOS and quantum conductance of the metallic (10,10) SWNT were first calculated within the framework of density-functional theory (DFT) using an *ab initio* pseudopotential method and a plane-wave basis set.[53] The DOS and conductance have shown quite different behavior than the prediction from the π-electron model. In the case of vacancies, the tight-binding model predicts the single DOS peak exactly at the Fermi level;[38,42,43,45,46,54] however, the electron-hole symmetry is no longer valid in the realistic calculation, and the position of the peak moves. Moreover, the two other narrow peaks originating from the broken σ bonds around the vacancy not found in the π-tight-binding model were obtained in the pseudopotential calculations. For the substitutional impurities and Stone-Wales defect, the DOS peaks are located away from the E_F too, and the conductance close to E_F is not significantly affected by the defects thus showing that the conductance at the E_F is quite robust with respect to the intratube local defects. According to similar *ab initio* pseudopotential calculations combined with the STM data, there is no significant modification of the π-band DOS due to B doping; the B-related acceptor states could only be detected in the σ band.[55] In this case, the observed prominent acceptorlike feature near the Fermi level and closing of band gap of the semiconducting tubes are explained in the terms of nanodomains of dopant islands but not by the isolated B substitutional atoms. Presumably, the N-donor structure is located around 0.35 eV above the Fermi level.[55] The DFT pseudopotential all-electron code with atom-centered numerical and plane-wave basis functions applied to vacancies in the armchair (n,n) $(n=4,6,8)$ and zigzag (10,0) SWNTs shows that the positions of vacancies states, their population, and electrical activity depend on the SWNTs diameter.[56] In the recent work,[33] the local DOS of the single, double, and triple vacancies, of the one and two adatoms on wall of tubule, of the vacancy/adatom complexes, as well as of the Stone-Wales defects in the semiconducting (10,0) SWNT were studied using virtually the same first-principles DFT technique. The results are compared with the low-temperature scanning tunneling microscopy and spectroscopy of the Ar^+-irradiated SWNTs. According to these data, in some cases, not the new states in gap can be observed due to the impacts of energetic ions, but changes in the local DOS in the valence and conduction bands only. On the contrary, other defects give rise to the single and double peaks in the band-gap region or complex multipeak configurations with nonzero intensity almost in the entire gap region. Finally, the pseudopotential supercell calculations for electric field dependence of the electronic and structural properties of the defective and radially deformed SWNTs are reported. The calculations show that band structure of the defective SWNTs varies quite differently on the applied electric field and strain from that of the perfect nanotubes.[57–59] The nonlinear elastic properties of the radially deformed and defective (8,0) tubule were also investigated recently.[60]

All the *ab initio* calculations have serious disadvantages because they were performed using a supercell model exhibiting a periodic arrangement of defects in the nanotube, the tubule with defects being arranged in a bulk periodic lattice. (As a typical example, the nanotubes composed of 2–6 unit cells and having 80–240 atoms were used for simulations of the (10,0) SWNT with defects in the recent work.[33]) The supercell calculations necessarily include interaction effects between the periodically arranged defects and tubules. Moreover, the chiral SWNTs have prohibitively large unit cells which made impossible simulations of defects in these tubules using the *ab initio* supercell models.[33] Finally, the ideas of the Green's function theory for electron structure of defects in the tubules were lost in the *ab initio* supercell calculations. The Green's function approach used already in the original π-electron models is more appropriate to treat the problem since it takes full advantage of the periodicity of the host SWNT structure and short range of the defect potential. Note that the Green's function method is widely used in the *ab initio* calculations of defects electronic structure in the bulk materials.[61–67]

In this paper, we present a method for treating the electronic structure of defects in the SWNTs which is generalization of a linear augmented cylindrical wave (LACW) theory of the perfect SWNTs band structure.[68–77] The method avoids using the supercell and superlattice geometries and combines the advantages of density-functional *ab initio* theory with the Green's function approach to the point defects electronic structure. The LACW method is just a reformulation for cylindrical multiatomic systems of the linear augmented plane-wave technique well known in the electronic-structure theory of bulk materials.[78–80] The account for the cylindrical geometry of the nanotubes in an explicit form offers the obvious advantages and is the main argument for using the cylindrical waves in the theory of nanotubes electronic structure. Here, we use the symmetry-adapted version of the LACW method in which one takes into account the rotational and helical symmetries of the ideal host SWNTs.[71] In this case, the cells contain only two carbon atoms, and the theory becomes applicable to any SWNT with point defects independent of the number of atoms in the translational unit cell of the host SWNTs. Previously, the LACW method was successfully used to correlate the structures of the ideal single-walled and double-walled carbon tubules with the their electron properties.

In Sec. II, we start from the short review of the LACW approach to the SWNT band-structure theory. Then, in the terms of the LACW technique, we calculate the Green's function of the perfect SWNT using a spectral representation. The Green's function of point impurity is evaluated in the terms of the matrix Dyson equation. The results for the local DOS of the boron and nitrogen impurities in the metallic, semimetallic, and semiconducting SWNTs and carbynes are presented in Sec. III. Finally, we discuss some of the limitations of such an approach and give conclusions.

II. THEORY

A. Structure of nanotubes

The perfect defect-free nanotubes can be constructed by rolling up a single graphite sheet. One can make such a seamless tubule without any special distortion of their bonding angles other than the introduction of curvature to the carbon hexagons through the rolling process. Each tubule can be labeled by the pair of integers (n_1,n_2), (where $n_1 \geq n_2 \geq 0$), which, together with C—C bond length $d_{\mathrm{C—C}}$, determine a geometry of the SWNTs. The perfect graphitic tubules defined by the integers (n_1,n_2) can also be defined in terms of their helical and rotational symmetries.[4,5] In order to construct the carbon SWNT, one has to map the first atom to an arbitrary point T_1 on the cylinder surface, which requires that the position of the second one T_2 be found by rotating this point,

$$\Phi_{T_2} = \pi \frac{n_1 + n_2}{n_1^2 + n_2^2 + n_1 n_2} \tag{1}$$

radians about the cylinder axis in conjunction with a translation,

$$\delta_{T_2} = \frac{d_{\mathrm{C—C}}}{2} \frac{n_1 - n_2}{(n_1^2 + n_2^2 + n_1 n_2)^{1/2}} \tag{2}$$

along this axis.

Let us map the first C atom to the point with cylindrical coordinates $Z_1=0$, $\Phi_1=0$, and $R_1=R_{NT}$. In this case, the cylindrical coordinates of the second C atom are $Z_2=\delta_{T_2}$, $\Phi_2=\Phi_{T_2}$, and $R_2=R_{NT}$, where

$$R_{NT} = \frac{d_{\mathrm{C—C}}\sqrt{3}}{2\pi}(n_1^2 + n_2^2 + n_1 n_2)^{1/2} \tag{3}$$

is the SWNTs radius.

The cylinder axis coincides with a C_ν rotational axis for the tubule, where ν is the largest common divisor of n_1 and n_2. Thus, the positions of these first two atoms can be used to locate $2(\nu-1)$ additional atoms on the cylinder surface by $(\nu-1)$ successive $2\pi/\nu$ rotations about the cylinder axis. Altogether, these 2ν atoms complete the specification of the helical motif that can then be used to tile the remainder of the tubule by repeated operation of a single screw operation $S(h,\omega)$ representing a translation,

$$h = \frac{3d_{\mathrm{C—C}}}{2} \frac{\nu}{(n_1^2 + n_2^2 + n_1 n_2)^{1/2}} = \frac{3\sqrt{3}d_{\mathrm{C—C}}^2}{4\pi} \frac{\nu}{R_{NT}} \tag{4}$$

along the cylinder axis in conjunction with a rotation,

$$\omega = 2\pi \frac{n_1 p_1 + n_2 p_2 + (n_2 p_1 + n_1 p_2)/2}{n_1^2 + n_2^2 + n_1 n_2} \tag{5}$$

radians about this axis. The angle ω is defined modulo 2π, the positive integers p_1 and p_2 are obtained from equation

$$p_2 n_1 - p_1 n_2 = \nu. \tag{6}$$

Thus, there are only two atoms in the minimum cell of the perfect SWNTs, and we can use two indices $\{n,\alpha\}$ to specify a particular carbon atom of the tubule, where n is the number of the two-atomic cell and $\alpha=1$ or 2.

In calculations of the SWNTs with substitutional boron and nitrogen impurities, we neglect a possible lattice relaxation in the defect regions because the covalent radii of the boron (0.82 Å) and nitrogen (0.75 Å) atoms differ not too much from that of the carbon (0.77 Å) and the SWNTs lattice is known to be very rigid. In this approximation, the atomic coordinates calculated above can be also used for the SWNTs with point impurities. Note that according to the pseudopotential data,[81] the equilibrium position of nitrogen atom is almost unchanged with respect to the corresponding C atoms in the undoped SWNTs, being moved by atmost 0.01 Å.

B. One-electron Hamiltonian and cylindrical muffin-tin potential

In the LACW method, a concept of one-electron orbitals is used, the separate electrons being characterized by wave functions of their own or spin orbitals. It is assumed that each spin orbital can be written as product of spatial and spin functions $\Psi_j(\mathbf{r})\alpha$ and $\Psi_j(\mathbf{r})\beta$, where α and β are the wave functions of electrons with spin "up" and "down," respectively. The spatial function $\Psi_j(\mathbf{r})$ is called an orbital. In the LACW method, the orbitals $\Psi_j(\mathbf{r})$, together with the corresponding one-electron energies E_j, are found by solving the one-electron Schrödinger equation,

$$\hat{H}\Psi_j(\mathbf{r}) = E_j\Psi_j(\mathbf{r}) \tag{7}$$

with effective one-electron Hamiltonian (in atomic Rydberg units)

$$\hat{H} = -\Delta + V(\mathbf{r}). \tag{8}$$

This Hamiltonian contains the kinetic-energy operator, $-\Delta$, and the operator $V(\mathbf{r})$ describing the summed action on the electron in consideration of all the other electrons in the system and all its nuclei.

In the LACW method, the approximations are made in the sense of muffin-tin (MT) potentials and local density-functional theory only. The electronic potential is spherically symmetrical in the $\Omega_{n\alpha}$ regions of MT spheres of atoms $\{n,\alpha\}$ and constant in the interspherical region Ω_{IS}. Inside these spheres, we calculate the electron potential by means of the local-density approximation with Slater exchange.[82–84] As usually, the radii of the MT spheres ($r_{MT}=d_{C—C}/2$) were chosen so that the atomic spheres touch but do not overlap; the sphere radius was kept the same for the carbon, boron, and nitrogen atoms. An infinite motion of an electron is obviously limited in the case of nanotubes by their size and shape. In terms of the LACW method, the atoms of nanotube are considered to be enclosed between two essentially impenetrable cylinder-shaped potential barriers Ω_a and Ω_b because there are two vacuum regions Ω_v on the outside and on the inside of the tubule. The radii a and b of these barriers are chosen so that the region confined by barriers accommodates a significant portion of the electron density of the tubule. As in our previous calculations of the perfect carbon SWNTs,[71] we take $a=R_{NT}+2.3$ and $b=R_{NT}-2.3$ a.u.

C. Symmetry of wave functions

In the perfect nanotube with the C_ν symmetry, the nuclei are arranged in a regular array described by a set of rotations by the angles $\omega_\nu t=(2\pi/\nu)t$ with arbitrary integer t. Therefore, we can introduce the discrete values of a wave vector $k_\Phi=\Lambda+\nu M$ corresponding to the periodic rotation operator and write using a cylindrical coordinate system Z,Φ,R,

$$\Psi(Z,\Phi+t\omega_\nu,R) = e^{i(\Lambda+\nu M)t\omega_\nu}\Psi(Z,\Phi,R), \tag{9}$$

where $M=0,\pm1,\ldots$ and $\Lambda=0,1,\ldots\nu-1$.

The perfect nanotube, being infinite in Z direction, is also invariant under the screw $\hat{S}(h,\omega)$ operation representing a translation h along this axis in conjunction with a rotation ω about it.[5] The screw transformations $\hat{S}(h,\omega)$ form an Abelian group isomorphous with the usual translation group $\hat{T}(h)$. Thus, according to Bloch's theorem, the wave function $\Psi(Z,\Phi,R)$ can be characterized by a continuous wave vector $K_P=k+k_P$,

$$\Psi(Z+th,\Phi+t\omega,R) = e^{i(k+k_P)th}\Psi(Z,\Phi,R). \tag{10}$$

Here, vectors k belong to the first one-dimensional Brillouin zone $-(\pi/h)<k\leq(\pi/h)$ and $k_P=2(\pi/h)P$, where $P=0,\pm1,\ldots$

Finally, in the LACW method, the one-electron eigenfunctions $\psi_\lambda(\mathbf{r}|\mathrm{k},\Lambda)$ of the ideal nanotube are written as the linear combinations of the basis functions $\Psi_{PMN}(\mathbf{r}|\mathrm{k},\Lambda)$,

$$\psi_\lambda(\mathbf{r}|\mathrm{k},\Lambda) = \sum_{PMN} a^\lambda_{PMN}(\mathrm{k},\Lambda)\Psi_{PMN}(\mathbf{r}|\mathrm{k},\Lambda). \tag{11}$$

Here, λ is a band index. The coefficients $a^\lambda_{PMN}(k,\Lambda)$ and corresponding energy eigenvalues $E_\lambda(k,\Lambda)$ are determined from a secular equation. The basis functions $\Psi_{PMN}(\mathbf{r}|\mathrm{k},\Lambda)$ and consequently $\psi_\lambda(\mathbf{r}|\mathrm{k},\Lambda)$ must satisfy the symmetry conditions (9) and (10).

D. Interspherical region

In the interspherical region of the nanotube, the basis functions $\Psi_{PMN}(\mathbf{r}|\mathrm{k},\Lambda)$ are the solutions of the Schrödinger equation,

$$\left\{-\left[\frac{1}{R}\frac{\partial}{\partial R}R\frac{\partial}{\partial R}+\frac{1}{R^2}\frac{\partial^2}{\partial\Phi^2}+\frac{\partial^2}{\partial Z^2}\right]+U(R)\right\}\Psi(Z,R,\Phi) = E\Psi(Z,R,\Phi). \tag{12}$$

Due to cylindrical symmetry of the potential $U(R)$,

$$U(R) = \begin{cases} 0 & b\leq R\leq a \\ \infty & R<b, R>a \end{cases}, \tag{13}$$

the solutions of Eq. (12) have the form[71]

$$E_{PMN}(k,\Lambda) = \left[k+k_P-(\Lambda+\nu M)\frac{\omega}{h}\right]^2+(\kappa_{|L+\nu M|,N})^2, \tag{14}$$

$$\Psi_{PMN}(\mathbf{r}|\mathrm{k},L)|_{\mathbf{r}\in\Omega_{IS}} = \frac{1}{\sqrt{2\pi h/\nu}}\exp i\left\{\left[\mathrm{k}+\mathrm{k}_P-(L+\nu M)\frac{\omega}{h}\right]Z+(L+\nu M)\Phi\right\} \times [C^{J,L}_{M,N}J_{L+\nu M}(\kappa_{|L+\nu M|,N}R)+C^{Y,L}_{M,N}Y_{L+\nu M}(\kappa_{|L+\nu M|,N}R)]. \quad (15)$$

Here, $J_{L+\nu M}$ and $Y_{L+\nu M}$ are the cylindrical Bessel functions of the first and second kinds, and N is a radial quantum number. The function $\Psi_{PMN}(\mathbf{r}|\mathrm{k},L)_{\mathbf{r}\in\Omega_{II}}$ should vanish at $R=a$ and $R=b$ and be normalized; these three conditions determine the $C^{J,\Lambda}_{M,N}$, $C^{Y,L}_{M,N}$, and $\kappa_{|\Lambda+\nu M|,N}$.[71] The function $\Psi_{PMN}(\mathbf{r}|\mathrm{k},L)_{\mathbf{r}\in\Omega_{II}}$ is referred as cylindrical wave; it corresponds to the free movement of electron in the infinite cylindrical layer with the C_ν rotational and $S(h,\omega)$ screw Z axis and satisfies the symmetry conditions (9) and (10).

E. MT region

Inside the MT sphere $\{n,\alpha\}$, in the local spherical coordinate system r,θ,φ, the basis functions $\Psi_{PMN}(\mathbf{r}|\mathrm{k},\Lambda)$ are expanded in spherical harmonics $Y_{lm}(\theta,\varphi)$,

$$\Psi_{n\alpha,PMN}(\mathbf{r}|\mathrm{k},\Lambda)|_{\mathbf{r}\in\Omega_{n\alpha}} = \sum_{l=0,}^{\infty}\sum_{m=-l}^{l}[A^{PMN}_{lm,n\alpha}(\mathrm{k},\Lambda)u^{n\alpha}_l(E^{n\alpha}_l,r) + B^{PMN}_{lm,n\alpha}(\mathrm{k},\Lambda)\dot{u}^{n\alpha}_l(E^{n\alpha}_l,r)]Y_{lm}(\hat{r}). \quad (16)$$

Here, $\hat{r}=(\theta,\varphi)$, $u^{n\alpha}_l$ is the solution of the radial Schrödinger equation,

$$\frac{1}{r}\frac{\partial^2}{\partial r^2}(ru^{n\alpha}_l)+\left[E^{n\alpha}_l-V_{n\alpha}(r)-\frac{l(l+1)}{r^2}\right]u^{n\alpha}_l=0 \quad (17)$$

for energy $E^{n\alpha}_l$, $\dot{u}^{n\alpha}_l(E^{n\alpha}_l,r)=\partial u^{n\alpha}_l(E^{n\alpha}_l,r)/\partial E^{n\alpha}_l$, and $V_{n\alpha}(r)$ is the local density spherically symmetric potential in the region of the MT sphere $\{n\alpha\}$. Inside the MT spheres with radius $r^{MT}_{n\alpha}$, the functions $u^{n\alpha}_l(r)$ are normalized, and the functions $\dot{u}^{n\alpha}_l(E^{n\alpha}_l,r)$ and $u^{n\alpha}_l(E^{n\alpha}_l,r)$ are orthogonal. Since the LACW wave functions are defined differently within the MT spheres and surrounding volume, the coefficients $A^{PMN}_{lm,n\alpha}(k,\Lambda)$ and $B^{PMN}_{lm,n\alpha}(k,\Lambda)$ in Eq. (16) are selected so that both the LACW $\Psi_{PMN}(\mathbf{r}|\mathrm{k},\Lambda)$ and its radial derivative have no discontinuities at the boundaries of the MT spheres.[68–70] Finally, in the region of the MT sphere $\{n\alpha\}$ with coordinates $\{Z_{n\alpha},\Phi_{n\alpha},R_{n\alpha}\}$, the basis function is written as[71]

$$\Psi_{PMN}(\mathbf{r}|\mathrm{k},\Lambda)|_{\mathbf{r}\in\Omega_{n\alpha}} = \frac{(r^{MT}_{n\alpha})^2}{\sqrt{2h/\nu}}(-1)^{(\Lambda+\nu M)}\exp i\left\{\left[\mathrm{k}+\mathrm{k}_P-(\Lambda+\nu M)\frac{\omega}{h}\right]Z_{n\alpha}+(\Lambda+\nu M)\Phi_{n\alpha}\right\} \times\sum_{m=-\infty}^{\infty}[C^{J,\Lambda}_{M,N}J_{m-(\Lambda+\nu M)}(\kappa_{|\Lambda+\nu M|,N}R_{n\alpha})+C^{Y,\Lambda}_{M,N}Y_{m-(\Lambda+\nu M)}(\kappa_{|\Lambda+\nu M|,N}R_{n\alpha})] \times\sum_{l=|m|}^{\infty}(-1)^{0.5(m+|m|)+l}i^l\left[\frac{(2l+1)(l-|m|)!}{(l+|m|)!}\right]^{1/2} \times[a^{PMN}_{lm,n\alpha}(r^{MT}_{n\alpha}|\mathrm{k},\Lambda)u^{n\alpha}_l(r,E^{n\alpha}_l)+b^{PMN}_{lm,n\alpha}(r^{MT}_{n\alpha}|\mathrm{k},\Lambda)\dot{u}^{n\alpha}_l(r,E^{n\alpha}_l)]Y_{lm}(\hat{r}). \quad (18)$$

The following notations have been used above:

$$a^{PMN}_{lm,\alpha}(r^{MT}_{n\alpha}|\mathrm{k},\Lambda)=I^{PMN}_{2,\alpha}(r^{MT}_{n\alpha}|\mathrm{k},\Lambda)\dot{u}_{l,\alpha}(r^{MT}_{n\alpha})-I^{PMN}_{1,\alpha}(r^{MT}_{n\alpha}|\mathrm{k},\Lambda)\dot{u}'_{l,\alpha}(r^{MT}_{n\alpha}), \quad (19)$$

$$b^{PMN}_{lm,\alpha}(r^{MT}_{n\alpha}|\mathrm{k},\Lambda)=I^{PMN}_{1,\alpha}(r^{MT}_{n\alpha}|\mathrm{k},\Lambda)u'_{l,\alpha}(r^{MT}_{n\alpha})-I^{PMN}_{2,\alpha}(r^{MT}_{n\alpha}|\mathrm{k},\Lambda)u_{l,\alpha}(r^{MT}_{n\alpha}), \quad (20)$$

where $u'_{l,n\alpha}=\partial u^{n\alpha}_l/\partial r$ and $\dot{u}'_{l,n\alpha}=\partial\dot{u}^{n\alpha}_l/\partial r$ are radial derivatives of the $u^{n\alpha}_l$ and $\dot{u}^{n\alpha}_l$ functions; I_1 and I_2 are integrals of the augmented Legendre polynomials $P^{|m|}_l$,

$$I_1=\int_{-\pi/2}^{\pi/2}\exp\left\{i\left[\left(k+k_P-(\Lambda+\nu M)\frac{\omega}{h}\right)r^{MT}_{n\alpha}\cos\theta\right]\right\}J_m(\kappa_{|\Lambda+\nu M|,N}r^{MT}_{n\alpha}\sin\theta)P^{|m|}_l(\cos\theta)\sin\theta d\theta, \quad (21)$$

$$I_2=\int_{-\pi/2}^{\pi/2}\exp\left\{i\left[\left(k+k_P-(\Lambda+\nu M)\frac{\omega}{h}\right)r^{MT}_{n\alpha}\cos\theta\right]\right\} \times\left[i\left(k+k_P-(\Lambda+\nu M)\frac{\omega}{h}\right)\cos\theta J_m(\kappa_{|\Lambda+\nu M|,N}r^{MT}_{n\alpha}\sin\theta)+(1/2)\kappa_{|\Lambda+\nu M|,N}\sin\theta\right] \times[J_{m-1}(\kappa_{|\Lambda+\nu M|,N}r^{MT}_{n\alpha}\sin\theta)-J_{m+1}(\kappa_{|\Lambda+\nu M|,N}r^{MT}_{n\alpha}\sin\theta)]P^{|m|}_l(\cos\theta)\sin\theta d\theta. \quad (22)$$

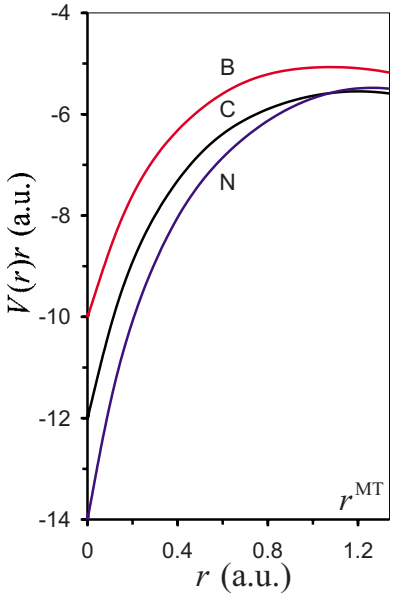

FIG. 1. (Color online) Radial dependence of the $V(r)r$ function in the region of MT spheres of the carbon, boron, and nitrogen atoms of the (5,5) SWNT. Here and in Fig. 2, Rydberg atomic units (a.u.) are used.

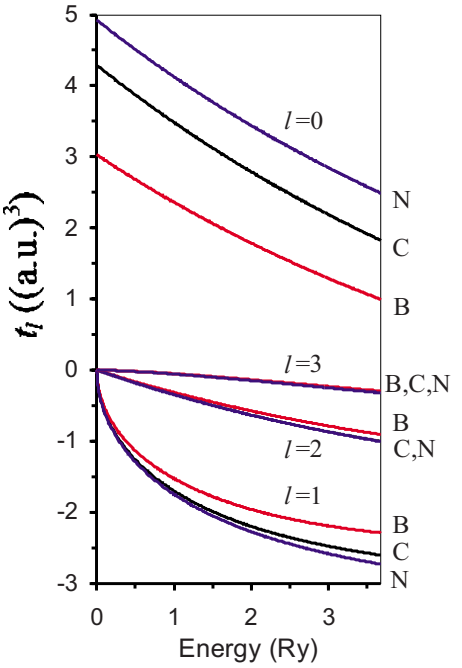

FIG. 2. (Color online) Energy dependence of the scattering t matrix of the carbon, boron, and nitrogen atoms of the (5,5) SWNT.

In angular momentum representation, one can determine a scattering t matrix,

$$t_l^{n\alpha}(E) = \int_0^{r_{n\alpha}^{MT}} j_l(\sqrt{E}r) V_{n\alpha}(r) u_l^{n\alpha}(r,E) r^2 dr \qquad (23)$$

for the potential $V_{n\alpha}(r)$. Moreover, in the linear methods,[78–80] one calculates the function $u_l^{n\alpha}(E,r)$ in the terms of exact solution $u_l^{n\alpha}(E_l^{n\alpha},r)$ and its energy derivative $\dot{u}_l^{n\alpha}(E_l^{n\alpha},r)$ at the fixed energy $E_l^{n\alpha}$,

$$u_l^{n\alpha}(E,r) = u_l^{n\alpha}(E_l^{n\alpha},r) + (E - E_l^{n\alpha})\dot{u}_l^{n\alpha}(E_l^{n\alpha},r). \qquad (24)$$

For (5,5) SWNT, Figs. 1 and 2 show the numerically calculated radial dependence of the potentials inside the spheres and an energy dependence of the scattering t matrices of the carbon, boron, and nitrogen atoms. The MT potential $V(r)$ decreases as one goes from the boron to carbon and from carbon to nitrogen and the product $V(r)r$ is equal to the nuclear charge at $r=0$. The MT spheres of the carbon, boron, and nitrogen spheres contain 3.62, 2.74, and 4.91 electrons, respectively.

F. One-electron Green's function

In the band-structure calculations, the solution of the one-electron Schrödinger Eq. (7) for the single-particle wave functions and corresponding energies represents the central problem. However, the calculation of the wave functions and energies can be avoided, if instead the single-particle Green's function $G(\mathbf{r},\mathbf{r}';E)$ which is the solution of the Schrödinger equation with a source at position $\mathbf{r}'$,

$$\{-\Delta + V(\mathbf{r}) - E\}G(\mathbf{r},\mathbf{r}';E) = -\delta(\mathbf{r}-\mathbf{r}') \qquad (25)$$

is determined.[66,85]

In terms of a complete set of the eigenfunctions $\Psi_j(\mathbf{r})$ corresponding to the eigenvalues E_j, the following spectral representation for the retarded Green's function can be obtained:

$$G(\mathbf{r},\mathbf{r}';E) = \sum_j \frac{\Psi_j(\mathbf{r})\Psi_j^*(\mathbf{r}')}{E - E_j + i\varepsilon}, \qquad (26)$$

representing, in the limit of Im $E=\varepsilon \to 0^+$, an outgoing wave at $\mathbf{r}$ with a source term at $\mathbf{r}'$. From the above equation and identity

$$\frac{1}{E - E_j + i\varepsilon} = -i\pi\delta(E - E_j) + \mathcal{P}\left(\frac{1}{E - E_j}\right), \qquad (27)$$

where $\mathcal{P}$ stands for the principal part, it follows that the expectation value of any physical quantity represented by an operator $\hat{A}$ can be harvested via the relation[66,85]

$$\langle A \rangle = -\frac{1}{\pi}\mathrm{Im}\int_{-\infty}^{E_F} \mathrm{Tr}[AG(E)]dE, \qquad (28)$$

if the matrix elements and trace in the right-hand side of this equation are calculated using the full basis set. Therefore, the Green's function contains all information which is given by the eigenfunctions, and if the Green's function can be computed, then all physical properties of the system can be found. Particularly, the imaginary part of $G(\mathbf{r},\mathbf{r};E)$ is directly related to the spectrally and space-resolved density of states,

$$\rho(\mathbf{r};E) = -\frac{1}{\pi}\mathrm{Im}\, G(\mathbf{r},\mathbf{r};E), \qquad (29)$$

and the local density of states

$$\rho_V(E) = -\frac{1}{\pi}\int_V \mathrm{Im}\, G(\mathbf{r},\mathbf{r};E)d\mathbf{r} \tag{30}$$

of a volume V is obtained by integrating over this volume. The real problem is the evaluation of the Green's function for the system of interest; in our case, it is the nanotube with point defect.

The equation for the Green's function $\tilde{G}(\mathbf{r},\mathbf{r};E)$ of the SWNT with impurity can be written as

$$\{\hat{H}-E\}\tilde{G}(\mathbf{r},\mathbf{r}';E) = -\delta(\mathbf{r}-\mathbf{r}') - \Delta V(\mathbf{r})\tilde{G}(\mathbf{r},\mathbf{r}';E). \tag{31}$$

Here, $\hat{H}$ is the Hamiltonian of the perfect SWNT and $\Delta V(\mathbf{r})=\tilde{V}(\mathbf{r})-V(\mathbf{r})$ is the difference between the potentials of the impurity and perfect tubules. It follows from this equation that the Green's function $\tilde{G}(\mathbf{r},\mathbf{r}';E)$ corresponding to the new Hamiltonian $\hat{H}+\Delta V(\mathbf{r})$ is related to the Green's function $G(\mathbf{r},\mathbf{r}';E)$ corresponding to $\hat{H}$ via the Dyson integral equation

$$\tilde{G}(\mathbf{r},\mathbf{r}';E) = G(\mathbf{r},\mathbf{r}';E) + \int G(\mathbf{r},\mathbf{r}'';E)\Delta V(\mathbf{r}'')\tilde{G}(\mathbf{r}'',\mathbf{r}';E)d\mathbf{r}''. \tag{32}$$

Most important is that the perturbed potential $\Delta V(\mathbf{r})$ is well localized near the impurity, while the perturbed wave functions $\tilde{\Psi}(\mathbf{r},\mathbf{r}';E)$ accurately described by the Lippmann-Schwinger equation

$$\tilde{\Psi}(\mathbf{r},\mathbf{r}';E) = \Psi(\mathbf{r},\mathbf{r}';E) + \int G(\mathbf{r},\mathbf{r}'';E)\Delta V(\mathbf{r}'')\tilde{\Psi}(\mathbf{r}'',\mathbf{r}';E)d\mathbf{r}'' \tag{33}$$

are not localized.

G. One-electron Green's function for array of MT spheres

Consider the Green's function of an array of spherically symmetric nonoverlapping potentials. The potential is given by

$$V(\mathbf{r}+\mathbf{R}_{n\alpha}) = V(Z+t_s h,\Phi+t_s\omega+t_\nu\omega_\nu) = V_{n\alpha}(\mathbf{r}), \tag{34}$$

$$t_s = 0,\pm 1,\pm 2,\ldots; \quad t_\nu = 0,1,\ldots,\nu-1, \tag{35}$$

and the Green's function is defined via

$$\{-\Delta + V_{n\alpha}(\mathbf{r}) - E\}G(\mathbf{r}+\mathbf{R}_{n\alpha},\mathbf{r}'+\mathbf{R}_{n'\alpha'};E) = -\delta_{n\alpha,n'\alpha'}\delta(\mathbf{r}-\mathbf{r}'). \tag{36}$$

In the mixed site angular momentum representation, by introducing the atom-centered coordinates, we can present the Green's function in the form of a series expansion based on the solutions of the Schrödinger equation in the MT spheres,[63–66,85–87]

$$G(\mathbf{r}+\mathbf{R}_{n\alpha},\mathbf{r}'+\mathbf{R}_{n'\alpha'};E) = -i\delta_{n,n'}\delta_{\alpha,\alpha'}\sqrt{E}\sum_L u_l^{n\alpha}(r_<,E)Y_L(\hat{\mathbf{r}})H_l^{n\alpha}(r_>,E)Y_L^*(\widehat{\mathbf{r}'}) + \sum_{L,L'} u_l^{n\alpha}(r,E)Y_L(\hat{\mathbf{r}})G_{L,L'}^{n\alpha,n'\alpha'}(E)u_{l'}^{n'\alpha'}(r',E)Y_{L'}^*(\widehat{\mathbf{r}'}). \tag{37}$$

Here, $\mathbf{R}_{n\alpha}$ and $\mathbf{R}_{n'\alpha'}$ are the positions of atoms α and α' in the cells n and n', respectively; $\mathbf{r}$ and $\mathbf{r}'$ restricted to the MT spheres $\{n,\alpha\}$ and $\{n',\alpha'\}$ are the local coordinate vectors of atoms $\{n,\alpha\}$ and $\{n',\alpha'\}$; $r_<=\min(r,r')$ and $r_>=\max(r,r')$; $L=(l,m)$ are the orbital quantum numbers; $G_{L,L'}^{n\alpha,n'\alpha'}(E)$ are the energy-dependent coefficients of the Green's function; $H_l^{n\alpha}(r,E)=u_l^{n\alpha}(r,E)+iN_l^{n\alpha}(r,E)$. Finally, the $u_l^{n\alpha}(r,E)$ is regular (converging at $r\to 0$) solution of the radial Schrödinger Eq. (17) and the $N_l^{n\alpha}(r,E)$ is irregular (diverging at $r\to 0$) solution of this equation.

In Eq. (37), the first term represents the Green's function for the scattering problem by the central potential in vacuum and the second one characterizes the effects of the nanotube structure. By construction, the expression in Eq. (37) for the Green's function satisfies in each MT sphere $\{n,\alpha\}$ the general solution of the Schrödinger Eq. (36) for the Green's function while the matrix $G_{L,L'}^{n\alpha,n'\alpha'}(E)$, the so-called structural Green's function, describes the connection of the solutions in the different spheres and thus contains all the information about the multiple-scattering problem, which is in this way reduced to the solution of an algebraic problem.

H. Structural Green's function

1. Perfect nanotube

Now, let us determine the coefficients of the Green's function $G_{L,L'}^{n\alpha,n'\alpha'}(E)$ for the perfect SWNT, the band structure and wave functions of the tubule being determined in the terms of the LACW method. Let us multiply the Eq. (37) by the $u_l^{n\alpha}(r,E)r^2drY_{L_1}^*(\hat{\mathbf{r}})d\hat{\mathbf{r}}$ and $u_{l'}^{n'\alpha'}(r',E)r'^2dr'Y_{L_2'}^*(\widehat{\mathbf{r}'})d\widehat{\mathbf{r}'}$ and integrate over MT regions of the atoms $\{n,\alpha\}$ and $\{n',\alpha'\}$. Then, we have

$$G_{L,L'}^{n\alpha,n'\alpha'}(E)\alpha_l^{n\alpha}(E)\alpha_{l'}^{n'\alpha'}(E) = i\delta_{n,n'}\delta_{\alpha,\alpha'}\delta_{L,L'}\sqrt{E}[\alpha_l^{n\alpha}(E)]^2 + \int_{\Omega_{n\alpha}}\int_{\Omega_{n'\alpha'}} G(\mathbf{r}+\mathbf{R}_{n\alpha},\mathbf{r}'+\mathbf{R}_{n'\alpha'},E)Y_L^*(\hat{\mathbf{r}})Y_{L'}(\widehat{\mathbf{r}'}) \times u_l^{n\alpha}(r,E)u_{l'}^{n'\alpha'}(r',E)r^2r'^2drdr'd\hat{\mathbf{r}}d\widehat{\mathbf{r}'}, \tag{38}$$

where

$$\alpha_l^{n\alpha}(E) = \int_0^{r_{n\alpha}^{MT}}[u_l^{n\alpha}(r,E)]^2r^2dr = 1+(E-E_l^{n\alpha})^2N_{l,\alpha}, \tag{39}$$

$$N_{l,\alpha} = \int_0^{r_{n\alpha}^{MT}} [\dot{u}_{l,\alpha}(E_l^{n\alpha}, r)]^2 r^2 dr. \tag{40}$$

In order to calculate the integral in Eq. (38), let us apply the spectral representation of Green's function

$$G(\mathbf{r},\mathbf{r}',E) = \frac{h}{2\pi}\sum_{\lambda}\sum_{\Lambda=0}^{\nu-1}\int_{-\pi/h}^{\pi/h}\frac{\psi_\lambda(\mathbf{r}|\mathrm{k},\Lambda)\psi_\lambda^*(\mathbf{r}'|\mathrm{k},\Lambda)}{E-E_\lambda(\mathrm{k},\Lambda)+i\varepsilon}d\mathrm{k}. \tag{41}$$

Substituting the wave functions [Eq. (18)] for $\mathbf{r}\in\Omega_{n\alpha}$ and $\mathbf{r}'\in\Omega_{n'\alpha'}$ in Eq. (41), we finally obtain

$$\begin{aligned}
G_{L,L'}^{n\alpha,n'\alpha'}(E) &= i\delta_{n,n'}\delta_{\alpha,\alpha'}\delta_{L,L'}\sqrt{E} + \frac{\nu(r_{n\alpha}r_{n'\alpha'})^2}{4\pi\alpha_l^{n\alpha}(E)\alpha_{l'}^{n'\alpha'}(E)} i^{l-l'}(-1)^{0.5(m+|m|+m'+|m'|)+l+l'} \\
&\times\left[\frac{(2l+1)(l-|m|)!(2l'+1)(l'-|m'|)!}{(l+|m|)!(l'+|m'|)!}\right]^{1/2}\sum_{PMN}\sum_{P'M'N''}(-1)^{\nu(M+M')}\sum_{\Lambda=0}^{\nu-1}\exp i[(\mathrm{k}_P-(\Lambda+\nu M)\omega/h)Z_{n\alpha} \\
&+(\Lambda+\nu M)\Phi_{n\alpha}]\exp\{-i[(\mathrm{k}_{P'}-(\Lambda+\nu M')\omega/h)Z_{n'\alpha'}+(\Lambda+\nu M')\Phi_{n'\alpha'}]\}[C_{M,N}^{J,\Lambda}J_{m-\Lambda-\nu M}(\kappa_{|\Lambda+\nu M|,N}R_{n\alpha}) \\
&+C_{M,N}^{Y,\Lambda}Y_{m-\Lambda-\nu M}(\kappa_{|\Lambda+\nu M|,N}R_{n\alpha})][C_{M',N'}^{J,\Lambda}J_{m'-\Lambda-\nu M'}(\kappa_{|\Lambda+\nu M'|,N'}R_{n'\alpha'})+C_{M',N'}^{Y,\Lambda}Y_{m'-\Lambda-\nu M'}(\kappa_{|\Lambda+\nu M'|,N'}R_{n'\alpha'})] \\
&\times\int_{-\pi/h}^{\pi/h}\exp[i\mathrm{k}(Z_{n\alpha}-Z_{n'\alpha'})][a_{lm,n\alpha}^{PMN}(r_{n\alpha}|\mathrm{k},\Lambda)+(E-E_l^{n\alpha})N_l^{n\alpha}b_{lm,n\alpha}^{PMN}(r_{n\alpha}|\mathrm{k},\Lambda)][a_{l'm',n'\alpha'}^{P'M'N'}(r_{n'\alpha'}|\mathrm{k},\Lambda) \\
&+(E-E_{l'}^{n'\alpha'})N_{l'}^{n'\alpha'}b_{l'm',n'\alpha'}^{P'M'N'}(r_{n'\alpha'}|\mathrm{k},\Lambda)]^*\sum_{\lambda}\left[-i\pi\delta[E-E_\lambda(\mathrm{k},\Lambda)]+\mathcal{P}\left(\frac{1}{E-E_\lambda(\mathrm{k},\Lambda)}\right)\right] \\
&\times a_{PMN}^{\lambda}(\mathrm{k},\Lambda)[a_{P'M'N'}^{\lambda}(\mathrm{k},\Lambda)]^* d\mathrm{k}.
\end{aligned} \tag{42}$$

2. Nanotube with impurity

Once the structural Green's function $G_{L,L'}^{n\alpha,n'\alpha'}(E)$ of the perfect SWNT is known, the Green's function for the nanotube with impurity can be evaluated in the terms of the matrix Dyson equation,[63–66]

$$\begin{aligned}
\tilde{G}_{L,L'}^{n\alpha,n'\alpha'}(E) &= G_{L,L'}^{n\alpha,n'\alpha'}(E) \\
&+\sum_{n'',\alpha''}\sum_{L''}G_{L,L''}^{n\alpha,n''\alpha''}(E)\Delta t_{l''}^{n''\alpha''}(E)\tilde{G}_{L'',L'}^{n''\alpha'',n'\alpha'}(E).
\end{aligned} \tag{43}$$

The $\Delta t_{l''}^{n''\alpha''}=\tilde{t}_{l''}^{n''\alpha''}-t_{l''}^{n''\alpha''}$ are the differences between the t matrices in the perturbed and perfect nanotubes determined by the perturbation of the potential well localized in the MT spheres of the impurity atoms. Since this difference is restricted to the vicinity of the impurity, the Green's function in this subspace can be easily determined in real space by matrix inversion. The rank of the matrices to be inverted is given by $n_d(l_{\max}+1)^2$; here, n_d is the number of perturbed MT potentials, and $l_{\max}$ is the maximum angular momentum used in the calculations. In this work, for the single impurities, we neglect the perturbation of the neighboring host atoms taking into account in Eq. (43) only the perturbation due to the impurity potential; this so-called single-site approximation is known to give a quite reasonable description of the electronic structure of the impurities in crystals.[63–66] Figure 2 shows that the absolute values of the scattering matrix elements perturbations $\Delta t_l^{\mathrm{B}}=\tilde{t}_l^{\mathrm{B}}-t_l^{\mathrm{C}}$ and $\Delta t_l^{\mathrm{N}}=\tilde{t}_l^{\mathrm{N}}-t_l^{\mathrm{C}}$ decrease strongly with increase in the angular momentum l. This results in a rapid convergence of the Green's function and finally of the electronic properties of the perturbed SWNTs. Particularly, $l_{\max}=2$ or even $l_{\max}=1$ give good convergence of the calculated electronic DOSs in the regions of impurities.

Substituting the structural function $\tilde{G}_{L,L'}^{n\alpha,n'\alpha'}(E)$ to Eq. (37), we can obtain the Green's function $\tilde{G}(\mathbf{r},\mathbf{r};E)$ for calculating a variety of the physical properties of the SWNT with impurity. In this work, we apply this approach to the particular case of the local electronic DOS corresponding to the MT region of the impurity atoms,

$$\rho_{MT,n\alpha}(E) = \frac{1}{\pi}\sum_{L}\alpha_l^{n\alpha}(E)[\sqrt{E}-\mathrm{Im}\,\tilde{G}_{L,L}^{n\alpha,n\alpha}(E)]. \tag{44}$$

III. RESULTS OF CALCULATIONS

Before tuning to the calculations of the SWNTs, let us look at the impurity-related levels in a carbyne, which is the most simple carbon nanowire with cylindrical symmetry.[88–91] The polyynic carbyne $(\mathrm{C}\text{—}\mathrm{C}\equiv\mathrm{C})_\infty$ is a linear chain of carbon atoms with alternating single and triple bonds equal to

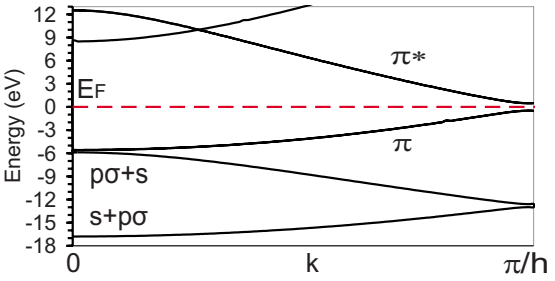

FIG. 3. (Color online) LACW band structure of polyynic carbyne. Here and below, energy relative to the Fermi level.

1.34 and 1.20 Å. The LACW band structure shows that the polyynic carbyne is a semiconductor with a direct energy gap E_g=0.98 eV (Fig. 3) in agreement with experimental data [1–2 eV (Ref. 88)].

Similar to the semiconducting SWNTs, the π bonding and π^* antibonding states of the polyynic carbyne form the top of valence and the bottom of conduction bands. Due to the high rotational symmetry of this structure, there is no mixing of the π states with low-lying p_σ and s bands. The local DOS in the carbon MT region of the perfect polyynic carbyne is visualized in Fig. 4 as the imaginary part of the Green's function calculated by the LACW method. (Note that there is no inner cylindrical cavity in this particular system; however, the LACW Green's function approach developed for the SWNTs can be easily adjusted to this more simple case of the nanorod geometry.)

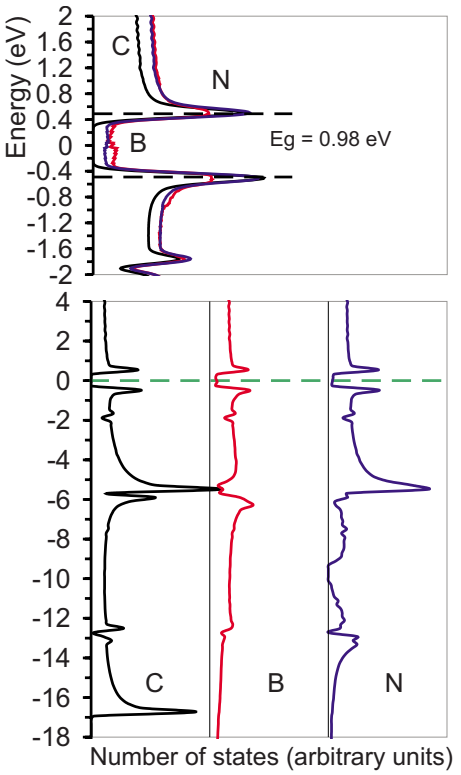

FIG. 4. (Color online) Local DOS of polyynic carbyne in the band-gap region (upper panel) and from the bottom of s band up to conduction band (lower panel). Here and below: perfect system (C), the boron (B), and nitrogen (N) impurities.

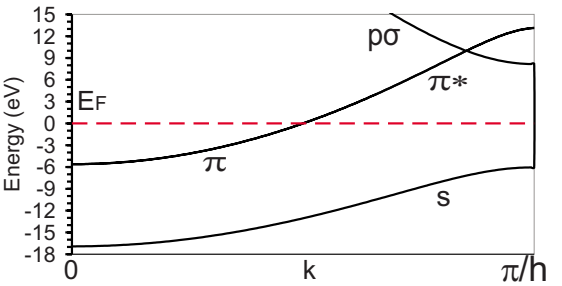

FIG. 5. (Color online) LACW band structure of cumulenic carbyne.

The local DOSs in the MT regions of the boron and nitrogen impurities of the doped polyynic carbyne calculated in the terms of the Dyson equation are plotted in this figure too. Both the boron and nitrogen impurities close the gap between the valence and conduction bands, the local DOS in this region being larger for the boron atom in comparison with the nitrogen one. The nitrogen impurity virtually does not influence the Van Hove singularities located at +0.5 and −0.5 eV relative to the Fermi energy and corresponding to the gap edges of the ideal system but the introduction of the boron atom results in decrease in these peaks. In addition to the states near the gap, the DOS of the perfect polyynic carbyne forms a double peak centered at −5.5 and −6 eV. In the case of the local DOS of boron impurity, there is not the peak but a well-defined dip in this region; for the nitrogen, a noticeable smoothing of the resonance is observed. The peak of the local DOS at −17 eV corresponding to the bottom of the s band is absent in the case of both impurities.

A cumulenic carbyne $(C{=}C)_\infty$ is a linear chain of carbon atoms with the double bonds equal to 1.27 Å; this polymorphic modification can be stabilized at high temperatures and pressures.[88–91] The cumulenic carbyne has the metallic band structure and DOS (Figs. 5 and 6). Similar to the case of metallic SWNTs, the Fermi level crosses the band separating

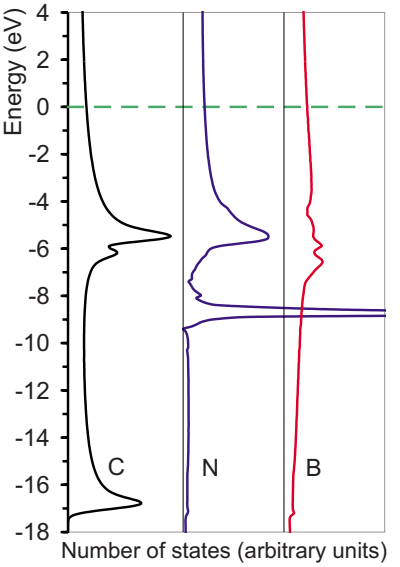

FIG. 6. (Color online) Local DOS of pure and B- and N-doped cumulenic carbyne.

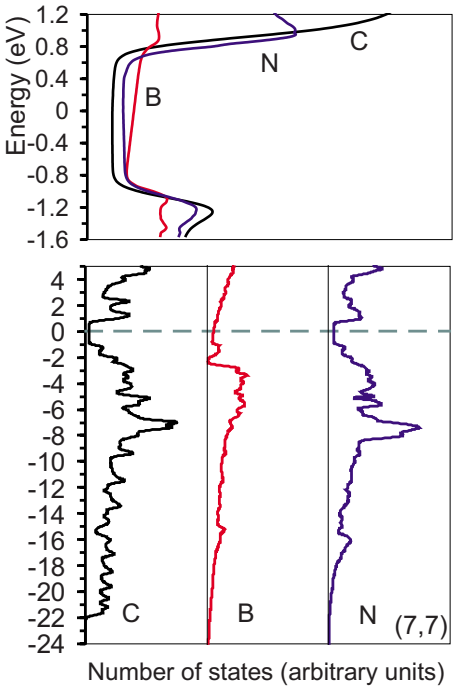

FIG. 7. (Color online) Local DOS of the perfect and B- and N-doped (7,7) SWNTs.

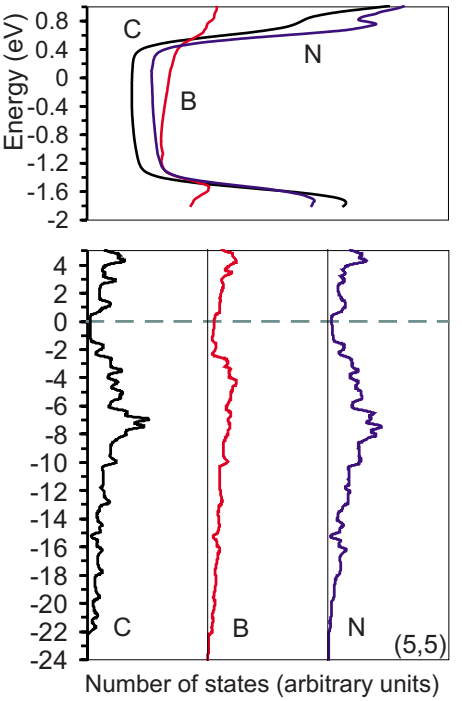

FIG. 8. (Color online) Local DOS of the perfect and B- and N-doped (5,5) SWNTs.

the low-energy bonding and high-energy antibonding π states. If the boron or nitrogen atom takes the place of carbon, the local DOS at the Fermi level increases in the 27% or 16%, respectively. Only the nitrogen defect gives rise to the new extremely narrow and high peak about −8.5 eV. A smearing of band between 4 and 7 eV specifies the effect of boron.

The SWNTs (13,0), (12,2), (11,3), (10,5), (9,6), and (8,7) have virtually equal diameters $d=10.15\pm0.15$ Å; the diameters $d=9.48$ and 10.70 Å of the SWNTs (7,7) and (12,4) are rather similar too. The SWNTs are known to be characterized by the "family index" $p=n_1-n_2$ mod 3. The tubules with $p=0$ are metallic or semimetallic, and those with $p=1$ and $p=2$ are semiconductors. Generally, the optical gap energies of the SWNTs with $p=1$ are somewhat larger than those of tubule with $p=2$.[75,92] Thus, there are the chiral and achiral, wide-gap and low-gap semiconducting, semimetallic, and metallic SWNTs in this representative series; moreover, the LACW band structures of all these tubules were already plotted in our previous work.[71] The SWNTs (5,5), (8,2), and (10,0) is another representative series with metallic, semimetallic, and semiconducting SWNTs with smaller diameters $d=7.41\pm0.42$ Å.

The purely carbon (7,7) SWNT with armchair geometry has a metallic electronic structure with constant DOS in the energy region between −0.7 and +0.7 eV relative to the Fermi level (Fig. 7). Close to the E_F, the electronic structure is significantly affected by the impurities. However, the boron and nitrogen defects do not destroy the metallic character of DOS. In this region, the main effect of the nitrogen impurity is about 50% virtually constant increase in the DOS; in the case of boron, there is further growth of the DOS. Comparison of these results with data for the small-diameter armchair (5,5) tubule (Fig. 8) shows that the impurity-induced perturbations of the DOSs are very similar independent of the diameter of armchair SWNTs.

The defect-free chiral (9,6) SWNT belongs to the semimetallic family, and there is no gap between the occupied and unoccupied states according the LACW band-structure data.[71] Moreover, due to the SWNT curvature effects, an overlap of the bonding and antibonding states equal to 0.15 eV takes place. In the DOS of the perfect tubule, this results in appearance of the peak exactly at E_F (Fig. 9). Upon the boron and nitrogen substitution, the local DOS in this region increases. The nitrogen impurity gives the largest DOS at E_F. The boron defect smoothens the three-peak structure between −0.5 and +0.5 eV. The perfect chiral (8,2) SWNT also belongs to the semimetallic family; however, in this case, a minigap with $E_g=0.15$ eV is formed because of the larger curvature of small-diameter tubule.[93] As a result, there is not peak but a dip in the DOS of ideal system (Fig. 10). The dip at the E_F retains in the DOS of both the boron and nitrogen dopants in spite of total increase in the local DOS in the region between −1.0 and +0.5 eV relative to the Fermi energy.

Figures 11–16 exhibit the influences of the boron and nitrogen impurities on the electronic DOSs of the six semiconducting SWNTs with the diameters of 10 Å and different chirality angles. For example, Figs. 15 and 16 show the data for the boron- and nitrogen-doped and perfect chiral (11,3) and (8,7) SWNTs having as many as 652 and 676 atoms in the translational unit cells. In all the semiconducting SWNTs, in the vicinity of optical gap, a drastic difference between the effects of the two types of impurities should be emphasized. The boron-related states clearly close but those of the nitrogen atoms do not close the gap of the perfect tubules. In the

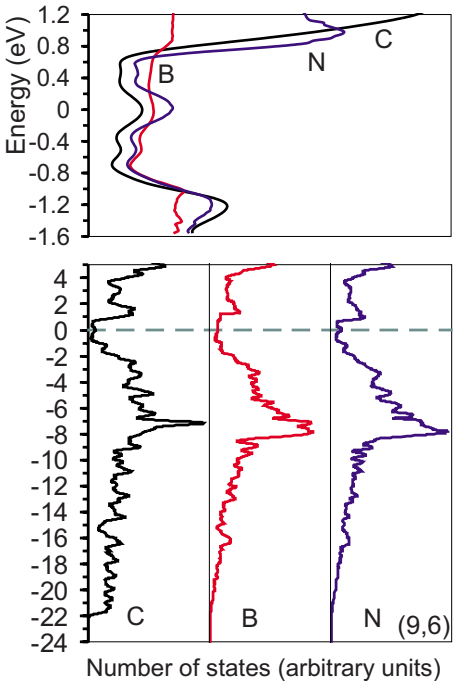

FIG. 9. (Color online) Local DOS of the perfect and doped (9,6) SWNTs.

gap region, the effects of nitrogen atom are restricted with a minor growth of the local DOSs just below and above the E_F. Figure 17 shows that this is also truth for the semiconducting small-diameter SWNT (10,0).

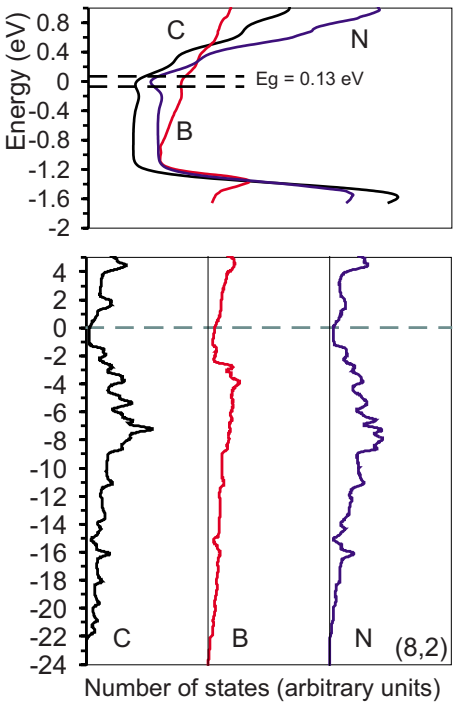

FIG. 10. (Color online) Local DOS of the perfect and doped (8,2) SWNTs. Here and below, the E_g values shown correspond to the perfect tubules and are derived from the LACW band-structure calculations (Ref. 71).

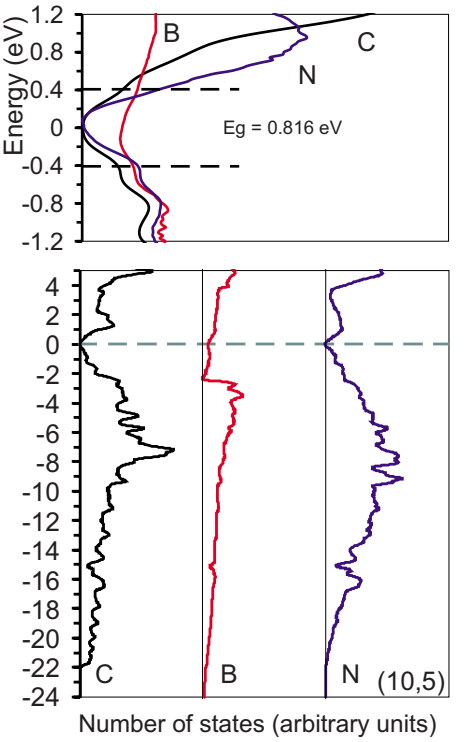

FIG. 11. (Color online) Local DOS of the perfect and doped (10,5) SWNTs.

Beyond the Fermi-energy region up to the *s* bottom of the valence bands, the effects of impurities are more or less similar in all the tubules. As one goes from carbon to the boron, the local DOS within the MT sphere decreases, and the peaks almost disappear. Generally, the effects of nitrogen defect are

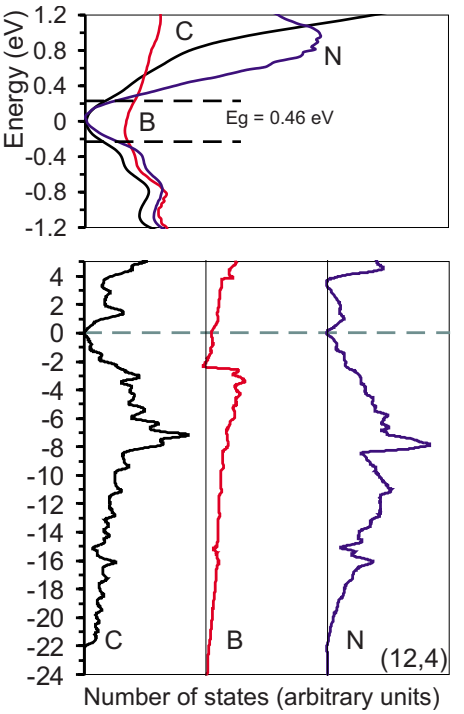

FIG. 12. (Color online) Local DOS of the perfect and doped (12,4) SWNTs.

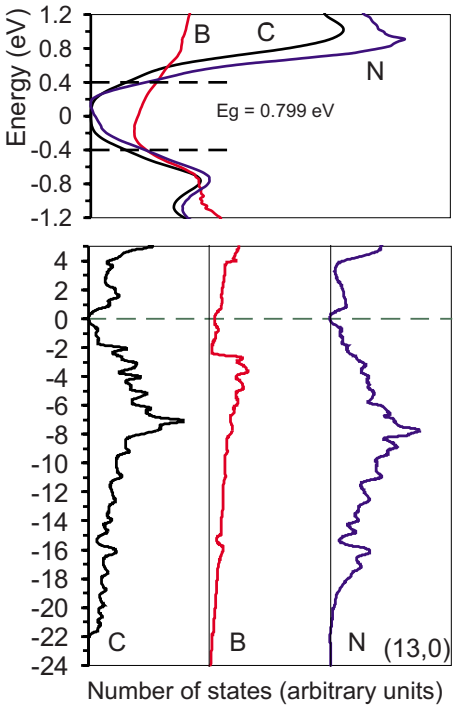

FIG. 13. (Color online) Local DOS of the perfect and doped (13,0) SWNTs.

opposite; the nitrogen local DOS is somewhat greater than that of the carbon, and there is no significant smoothing of the DOS picture.

It would be very interesting to compare the results of the Green's function LACW technique designed for a single defect to those obtained by the usual supercell plane-wave pseudopotential DFT method for array of impurities. Unfortunately, the possibilities of this comparison are greatly limited because there are the pseudopotential calculations of the achiral nanotubes only. (The unit cells of the chiral SWNTs contain too many atoms for the plane-wave pseudopotential

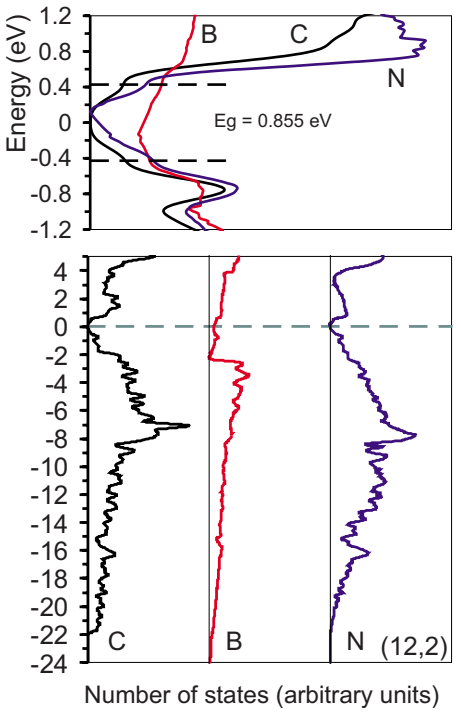

FIG. 14. (Color online) Local DOS of the perfect and doped (12,2) SWNTs.

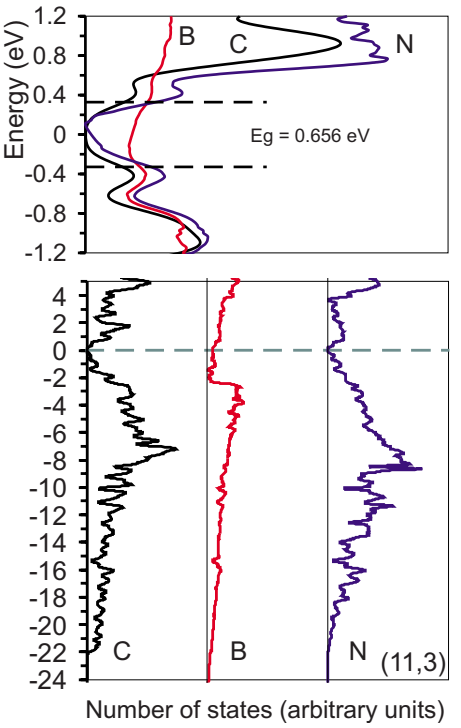

FIG. 15. (Color online) Local DOS of the perfect and doped (11,3) SWNTs.

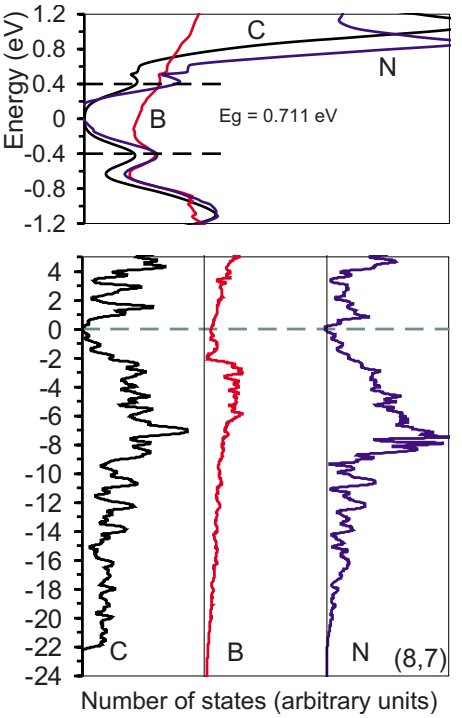

FIG. 16. (Color online) Local DOS of the perfect and doped (8,7) SWNTs.

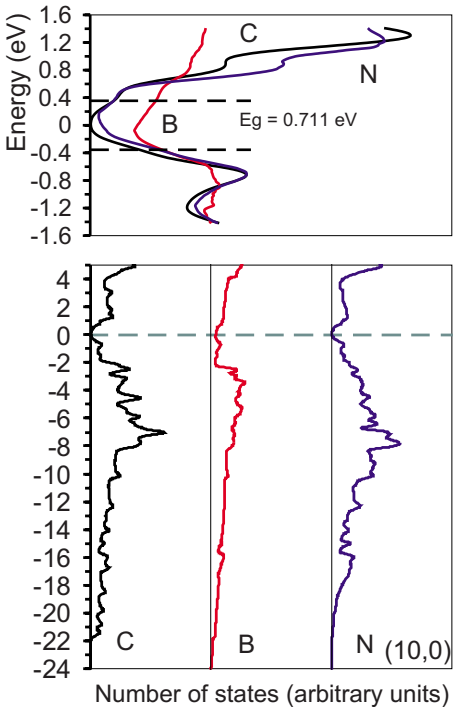

FIG. 17. (Color online) Local DOS of the perfect and doped (10,0) SWNTs.

method which suffers from a slow convergence and an unfavorable scaling: the number of basis functions and time taken to perform such a calculation on a computer increases asymptotically with the cube of the number of atoms in the cell.[94])

For example in paper,[53] the electronic structure of the (10,10) SWNT with boron and nitrogen impurities was calculated in the terms of the *ab initio* plane-wave nonlocal pseudopotential method, the supercell of 10–20 Å in each direction being used. Figure 18 shows the local DOSs for the Fermi-energy region of the boron- and nitrogen-doped (10,10) SWNTs calculated using this approach together with the Green's function LACW data. The overall structures of the local DOSs are similar; particularly, both methods predict that introduction of impurities does not result in a formation of the forbidden gaps. However, there are important differences. The pseudopotential calculation of the local DOS around the boron impurity predicts a double peak with maximums at −0.7 and −0.8 eV below the Fermi level as well as a sharp peak above this level at 0.75 eV. In the pseudopotential local DOS of the nitrogen impurity, a position of these bands is opposite to the boron case, the double-peak band is located above and a single peak below Fermi level. Note that a form of all these bands having very sharp edges is typical for the Van Hove singularities in the one-dimensional periodic systems. This seems to be an artifact of theory determined by the interaction of defects in supercell geometry used. It is pointed in the paper[53] that spatial extent of the wave functions corresponding to the impurity-related bound states with energies of −0.7 and 0.5 eV for boron and nitrogen impurities equals to 10 Å; the spatial extent of the wave functions corresponding to the states with binding energies equal to −0.8 eV and +0.8 eV for the boron and nitrogen is roughly 200 Å and 50 Å, respectively. Thus, the delocalization of functions is strong enough to guarantee a coupling between the neighbor impurities. The double-peak structures in the local DOSs of impurities can be understood as the bonding and antibonding combinations of the impurity orbitals. In the Green's function LACW DOSs, one observes the analogous bands located in the same energy regions as in the case of the plane-wave pseudopotential theory but the bands are obviously broadened and their splitting disappears as it is

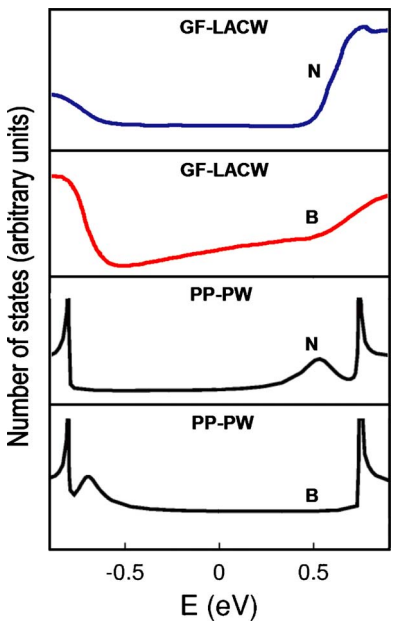

FIG. 18. (Color online) Local DOSs of the doped (10,10) SWNT calculated using the plane-wave pseudopotential and Green's function LACW methods.

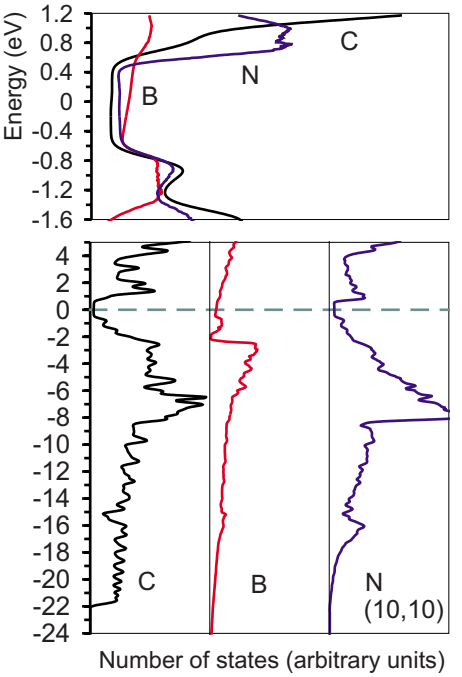

FIG. 19. (Color online) LACW local DOS of the perfect and doped (10,10) SWNTs.

expected for the single impurity. Finally, it is to be noted that the plane-wave pseudopotential calculations are restricted with a vicinity of the Fermi level but the LACW approach permits calculating the electronic structure in a wide energy range from the conduction band up to the bottom of the valence *s* band (Fig. 19).

IV. CONCLUDING REMARKS

We have developed the distinct method for the realistic theoretical studies of electronic structure of the SWNTs with point defects and performed calculations of local DOS for the substitutional boron and nitrogen impurities in the variety of the SWNTs. The calculations are based on the linear augmented cylindrical wave Green's function method and the local-density functional and muffin-tin approximations for the electronic potential. It is of great importance that the *ab initio* method is developed which is applicable to any SWNT including the chiral ones with very large translational unit cells. The method realized in the terms of the single-site approximation can be extended to the cases where the potentials of the neighboring atoms are also disturbed and the atomic structure relaxations are allowed.

ACKNOWLEDGMENTS

The work was performed in frames of Russian Scientific and Research Program "Scientific and pedagogic personal for innovations in Russia in 2009-2013 years." This work was supported by Russian Basic Research Foundation (Grant No. 08-03-00262).

*dima@lester.ru

[1] R. Saito, M. Fujita, G. Dresselhaus, and M. S. Dresselhaus, Phys. Rev. B **46**, 1804 (1992).
[2] R. Saito, M. Fujita, G. Dresselhaus, and M. S. Dresselhaus, Appl. Phys. Lett. **60**, 2204 (1992).
[3] N. Hamada, S. I. Sawada, and A. Oshiyama, Phys. Rev. Lett. **68**, 1579 (1992).
[4] J. W. Mintmire, B. I. Dunlap, and C. T. White, Phys. Rev. Lett. **68**, 631 (1992).
[5] C. T. White, D. H. Robertson, and J. W. Mintmire, Phys. Rev. B **47**, 5485 (1993).
[6] T. W. Ebbesen, Phys. Today **49**(6), 26 (1996).
[7] C. Dekker, Phys. Today **52**(5), 22 (1999).
[8] S. J. Tans, M. H. Devoret, R. J. A. Groeneveld, and C. Dekker, Nature (London) **386**, 474 (1997).
[9] S. J. Tans, A. R. M. Verschueren, and C. Dekker, Nature (London) **393**, 49 (1998).
[10] H. W. Ch. Postma, T. Teepen, Z. Yao, M. Grifoni, and C. Dekker, Science **293**, 76 (2001).
[11] J. Kong, N. R. Franklin, C. Zhou, M. G. Chapline, S. Peng, K. Cho, and H. Dai, Science **287**, 622 (2000).
[12] A. Modi, N. Koratkar, E. Lass, B. Wei, and P. M. Ajayan, Nature (London) **424**, 171 (2003).
[13] K. Jensen, J. Weldon, H. Garcia, and A. Zettl, Nano Lett. **7**, 3508 (2007).
[14] K. Jensen, K. Kim, and A. Zettl, Nat. Nanotechnol. **3**, 533 (2008).
[15] L. Xiao, Z. Chen, C. Feng, L. Liu, Z.-Q. Bai, Y. Wang, L. Qian, Y. Zhang, Q. Li, K. Jiang, and S. Fan, Nano Lett. **8**, 4539 (2008).
[16] M. Rinkiö, A. Johansson, G. S. Paraoanu, and P. Torma, Nano Lett. **9**, 643 (2009).
[17] F. Kuemmeth, S. Ilani, D. C. Ralph, and P. L. McEuen, Nature (London) **452**, 448 (2008).
[18] Y. Fan, B. R. Goldsmith, and P. G. Collins, Nature Mater. **4**, 906 (2005).
[19] A. V. Krasheninnikov and F. Banhart, Nature Mater. **6**, 723 (2007).
[20] A. Hashimoto, K. Suenaga, A. Gloter, K. Urita, and S. Iijima, Nature (London) **430**, 870 (2004).
[21] Z. Osváth, G. Vértesy, L. Tapasztó, F. Wéber, Z. E. Horváth, J. Gyulai, and L. P. Biró, Mater. Sci. Eng., C **26**, 1194 (2006).
[22] Z. Osváth L. Tapasztó, G. Vértesy, A. A. Koós, Z. E. Horváth, J. Gyulai, and L. P. Biró, Phys. Status Solidi A **204**, 1825 (2007).
[23] J. Kotakoski, A. V. Krasheninnikov, Y. Ma, A. S. Foster, K. Nordlund, and R. M. Nieminen, Phys. Rev. B **71**, 205408 (2005).
[24] M. Berthe, S. Yoshida, Y. Ebine, K. Kanazawa, A. Okada, A. Taninaka, O. Takeuchi, N. Fukui, H. Shinohara, S. Suzuki, K. Sumitomo, Y. Kobayashi, B. Grandidier, D. Stiévenard, and H. Shigekawa, Nano Lett. **7**, 3623 (2007).
[25] M. Bockrath, W. Liang, D. Bozovic, J. H. Hafner, C. M. Lieber, M. Tinkham, and H. Park, Science **291**, 283 (2001).
[26] T. W. Odom, J.-L. Huang, C. L. Cheung, and C. M. Lieber, Science **290**, 1549 (2000).
[27] J. A. Robinson, E. S. Snow, S. C. Bădescu, T. L. Reinecke, and F. K. Perkins, Nano Lett. **6**, 1747 (2006).
[28] M. C. Gordillo, Phys. Rev. Lett. **96**, 216102 (2006).
[29] L. Sun, F. Banhart, A. V. Krasheninnikov, J. A. Rodríguez-Manzo, M. Terrones, and P. M. Ajayan, Science **312**, 1199 (2006).
[30] M. K. Kostov, E. E. Santiso, A. M. George, K. E. Gubbins, and M. Buongiorno Nardelli, Phys. Rev. Lett. **95**, 136105 (2005).
[31] I. Fenoglio, G. Greco, M. Tomatis, J. Muller, E. Raymundo-Pinero, F. Béguin, A. Fonseca, J. Nagy, D. Lison, and B. Fubini, Chem. Res. Toxicol. **21**, 1690 (2008).
[32] L. Tapasztó, P. Nemes-Incze, Z. Osváth, M. C. Bein, Al. Darabont, and L. P. Biró, Physica E **40**, 2263 (2008).
[33] A. Tolvanen, G. Buchs, P. Ruffieux, P. Gröning, O. Gröning, and A. V. Krasheninnikov, Phys. Rev. B **79**, 125430 (2009).
[34] I. O. Maciel, N. Anderson, M. A. Pimenta, A. Hartschuh, H. Qian, M. Terrones, H. Terrones, J. Campos-delgado, A. M. Rao, L. Novotny, and A. Jorio, Nature Mater. **7**, 878 (2008).
[35] M. Freitag, Nature Mater. **7**, 840 (2008).
[36] A. V. Krasheninnikov, in *Chemistry of Carbon Nanotubes*, edited by V. A. Basiuk and E. V. Basiuk (Blackwell, Oxford, 2007).
[37] J.-C. Charlier, T. W. Ebbesen, and P. Lambin, Phys. Rev. B **53**,

11108 (1996).
[38] L. Chico, L. X. Benedict, S. G. Louie, and M. L. Cohen, Phys. Rev. B **54**, 2600 (1996).
[39] L. Chico, V. H. Crespi, L. X. Benedict, S. G. Louie, and M. L. Cohen, Phys. Rev. Lett. **76**, 971 (1996).
[40] V. H. Crespi, M. L. Cohen, and A. Rubio, Phys. Rev. Lett. **79**, 2093 (1997).
[41] L. Chico, M. P. Lopez Sancho, and M. C. Muñoz, Phys. Rev. Lett. **81**, 1278 (1998).
[42] T. Kostyrko, M. Bartkowiak, and G. D. Mahan, Phys. Rev. B **59**, 3241 (1999).
[43] T. Kostyrko, M. Bartkowiak, and G. D. Mahan, Phys. Rev. B **60**, 10735 (1999).
[44] Ph. Lambin, A. Fonseca, J. P. Vigneron, J. B. Nagy, and A. A. Lucas, Chem. Phys. Lett. **245**, 85 (1995).
[45] M. Igami, T. Nakanishi, and T. Ando, J. Phys. Soc. Jpn. **68**, 716 (1999).
[46] H. J. Choi and J. Ihm, Solid State Commun. **111**, 385 (1999).
[47] N. Neophytou, S. Ahmed, and G. Klimeck, Appl. Phys. Lett. **90**, 182119 (2007).
[48] A. Krasheninnikov, Solid State Commun. **118**, 361 (2001).
[49] A. V. Krasheninnikov, K. Nordlund, M. Sirviö, E. Salonen, and J. Keinonen, Phys. Rev. B **63**, 245405 (2001).
[50] T. Ando, T. Nakanishi, and M. Igami, J. Phys. Soc. Jpn. **68**, 3994 (1999).
[51] T. Ando, J. Phys. Soc. Jpn. **74**, 777 (2005).
[52] T. Nakanishi and T. Ando, J. Phys. Soc. Jpn. **68**, 561 (1999).
[53] H. J. Choi, J. Ihm, S. G. Louie, and M. L. Cohen, Phys. Rev. Lett. **84**, 2917 (2000).
[54] M. P. Anantram and T. R. Govindan, Phys. Rev. B **58**, 4882 (1998).
[55] D. L. Carroll, Ph. Redlich, X. Blase, J.-C. Charlier, S. Curran, P. M. Ajayan, S. Roth, and M. Rühle, Phys. Rev. Lett. **81**, 2332 (1998).
[56] J. M. Carlsson, Phys. Status Solidi B **243**, 3452 (2006).
[57] L.-G. Tien, C.-H. Tsai, F.-Y. Li, and M.-H. Lee, Phys. Rev. B **72**, 245417 (2005).
[58] Y. V. Shtogun and L. M. Woods, J. Phys. Chem. C **113**, 4792 (2009).
[59] Y. V. Shtogun and L. M. Woods, Carbon **47**, 3252 (2009).
[60] Y. V. Shtogun and L. M. Woods, J. Appl. Phys. **107**, 061803 (2010).
[61] A. M. Clogston, Phys. Rev. **125**, 439 (1962).
[62] J. L. Beeby, Proc. R. Soc. London, Ser. A **302**, 113 (1967).
[63] R. Zeller and P. H. Dederichs, Phys. Rev. Lett. **42**, 1713 (1979).
[64] P. J. Braspenning, R. Zeller, A. Lodder, and P. H. Dederichs, Phys. Rev. B **29**, 703 (1984).
[65] V. S. Stepanyuk, A. Szasz, A. A. Katsnelson, A. V. Kozlov, and O. V. Farberovich, Z. Phys. B: Condens. Matter **81**, 391 (1990).
[66] P. H. Dederichs, S. Lounis, and R. Zeller, in *Computational Nanoscience: Do It Yourself!*, NIC Series Vol. 31, edited by J. Grotendorst, S. Blügel, and D. Marx (John von Neumann Institute for Computing, Jülich, 2006), p. 279.
[67] O. V. Farberovich, A. Yaresko, K. Kikoin, and V. Fleurov, Phys. Rev. B **78**, 085206 (2008).
[68] P. N. D'yachkov, O. M. Kepp, and A. V. Nikolaev, Dokl. Chem. **365**, 67 (1999); *Science and Application of Nanotubes*, edited by D. Tomanek and R. J. Enbody (Kluwer Academic/Plenum. New York, 2000), p. 77.
[69] P. N. D'yachkov and D. V. Kirin, Dokl. Phys. Chem. **369**, 326 (1999); in *Proceedings of the School and Workshop Nanotubes and Nanostructures*, Santa Margherita di Pula, CA, Italy, 2000, edited by S. Bellucci (SIF, Bologna, 2001) [Ital. Phys. Soc., Conf. Proc. 74, 203 (2000)].
[70] P. N. D'yachkov, in *Encyclopedia of Nanoscience and Nanotechnology*, edited by H. S. Nalwa (American Scientific, Valencia, CA, 2004), Vol. 1, p. 192.
[71] P. N. D'yachkov and D. V. Makaev, Phys. Rev. B **76**, 195411 (2007).
[72] P. N. D'yachkov and D. V. Makaev, Phys. Rev. B **74**, 155442 (2006).
[73] P. N. D'yachkov and D. V. Makaev, Phys. Rev. B **71**, 081101(R) (2005).
[74] P. N. D'yachkov, H. Hermann, and D. V. Kirin, Appl. Phys. Lett. **81**, 5228 (2002).
[75] P. N. D'yachkov and H. Hermann, J. Appl. Phys. **95**, 399 (2004).
[76] P. N. D'yachkov and D. V. Makaev, Phys. Status Solidi B **246**, 140 (2009).
[77] P. N. D'yachkov and D. V. Makaev, J. Phys. Chem. Solids **70**, 180 (2009).
[78] O. K. Andersen, Phys. Rev. B **12**, 3060 (1975).
[79] D. D. Koelling and G. O. Arbman, J. Phys. F: Met. Phys. **5**, 2041 (1975).
[80] D. J. Singh, *Planewaves, Pseudopotentials and the LAPW Method* (Kluwer, Boston, 1994).
[81] A. H. Nevidomskyy, G. Csányi, and M. C. Payne, Phys. Rev. Lett. **91**, 105502 (2003).
[82] J. C. Slater, *The Self-Consistent Field for Molecules and Solids*, Quantum Chemistry of Molecules and Crystals (McGraw-Hill, New York, 1974), Vol. 4.
[83] P. Hohenberg and W. Kohn, Phys. Rev. **136**, B864 (1964).
[84] W. Kohn and L. J. Sham, Phys. Rev. **140**, A1133 (1965).
[85] P. Mavropoulos and N. Papanikolaou, in *Computational Nanoscience: Do It Yourself!*, NIC Series Vol. 31, edited by J. Grotendorst, S. Blügel, and D. Marx (John von Neumann Institute for Computing, Jülich, 2006), p. 131.
[86] J. Korringa, Physica (Amsterdam) **13**, 392 (1947).
[87] W. Kohn and N. Rostoker, Phys. Rev. **94**, 1111 (1954).
[88] Yu. P. Kudryavtsev, S. E. Evsyukov, M. B. Guseva, V. G. Babaev, and V. V. Khvostov, Izv. Akad. Nauk., Ser. Khi. **3**, 450 (1993) [Russ. Chem. Bull. **42**, 399 (1993) (Engl. Transl.)].
[89] T. D. Varfolomeeva, S. V. Popova, A. G. Lyapin, V. V. Brazhkin, and R. A. Sadykov, Inorg. Mater. **41**, 950 (2005).
[90] J. A. Lenz, C. A. Perottoni, N. M. Balzaretti, and J. A. H. da Jornada, J. Appl. Phys. **89**, 8284 (2001).
[91] R. H. Baughman, Science **312**, 1009 (2006).
[92] S. M. Bachilo, M. S. Strano, C. Kittrell, R. H. Hauge, R. E. Smalley, and R. B. Weisman, Science **298**, 2361 (2002).
[93] M. Ouyang, J.-L. Huang, C. Li, and C. M. Lieber, Science **292**, 702 (2001).
[94] C.-K. Skylaris, P. D. Haynes, A. Mostofi, and M. C. Payne, J. Chem. Phys. **122**, 084119 (2005).